Direct Measurement of the Mass Transport Coefficient of Water in Silica-Gel Using the Zero Length Column Technique

Direct Measurement of the Mass Transport Coefficient of Water in Silica-Gel Using the Zero Length Column Technique.

Stefano Brandani* and Enzo Mangano
School of Engineering, University of Edinburgh, Edinburgh, EH9 3FB, UK

Abstract

In all silica-gel adsorption processes driven by low-grade heat, the kinetics of adsorption of water on silica-gel is very important in order to optimize design and becomes an essential factor in ultra-low grade heat applications. A new approach for the determination of the mass transfer coefficient of water in commercial silica-gel is proposed and demonstrated with measurements on a single particle using the zero length column technique. Under equilibrium conditions the methodology offers the key advantage to acquire equilibrium isotherms with thousands of points in less than one day. This allows to obtain the relationship between vapour concentration and equilibrium adsorbed amount through numerical interpolation. At higher flowrates, the system operates under kinetic control therefore allowing the determination of the mass transfer coefficient. The novel approach calculates all the elements needed to obtain the mass transfer coefficient from the measured signals without the need to use a specific model. Adsorption and desorption experiments were carried out at different flowrates and three different temperatures. The kinetic responses can be used to determine an average mass transfer coefficient, which is consistent with literature values, but a complex behaviour is observed with surface diffusion as the main contribution to the transport process.

Keywords: Adsorption kinetics; Water; Silica-gel; Zero length column.

* Corresponding author: s.brandani@ed.ac.uk

Introduction

Adsorption of water on silica-gel is at the basis of several heat-driven applications aimed at improving energy efficiency including for example: adsorption desalination [1]; adsorptive heat storage [2,3]; adsorption chillers [4,5]; and desiccant wheels [6,7]. To develop a dynamic model of these processes it is essential to have accurate equilibrium isotherms and determine mass transfer coefficients, but measuring these properties for water is a challenge. Volumetric and gravimetric commercial systems are available to determine individual points on isotherms and are time consuming experiments [8–12]. Mass transfer coefficients are then measured using a variety of techniques which require combined heat and mass transfer models [13–16], in addition to a suitable form of isotherm model which has to also capture accurately the adsorption energy, as the experiments are performed under non-isothermal conditions. With mesoporous materials such as silica-gel there is also the added complication that the isotherm exhibits a hysteresis loop leading to difficulties in representing correctly adsorption and desorption kinetics. For example [17] correlate water adsorption/desorption kinetics in a chromatographic column using different concentration dependent parameters for the two branches, leading to an overall kinetic model with 10 parameters to be determined. Concentration frequency response [15] has been shown to provide accurate values of mass transfer coefficients at specific concentrations and a full concentration dependence study would be time consuming. Furthermore, when the measurement is carried out in the hysteresis loop the coefficients correspond to trajectories on the scanning curves and not the main adsorption and desorption branches [15]. There is therefore the need for a simple technique that allows to determine mass transfer coefficients for water over the entire concentration range, in both adsorption and desorption steps.

The aim of this contribution is to demonstrate the use of the zero length column (ZLC) technique [18,19] for measuring mass transfer coefficients for the system water/silica-gel. The key innovation lies in several important features:

1. Low flowrate experiments can be used to determine the accurate shape of the adsorption isotherm as the ZLC generates thousands of equilibrium points and as a result no model is needed to obtain the relationship between vapour concentration and equilibrium adsorbed amount;
2. The small samples used in a ZLC, typically at least 3 orders of magnitude less than a normal chromatographic column, ensures near isothermal conditions considering also that all of the gas flows through the ZLC thus providing convective heat transfer in addition to the conduction to the comparatively large mass of steel surrounding the sample;

3. The measured vapour concentration can be converted to the adsorbed phase concentration applying the column mass balance [18], thus all quantities needed to determine the mass transfer coefficient are available;
4. Single beads or fragments can be used ensuring no bed/layer effects and negligible pressure drops, leading to a system that is easy to represent;
5. The methodology to be used is very different from the traditional approach of matching the kinetic response under dilute conditions [18,19] in desorption only mode. In fact both adsorption and desorption kinetics under large concentration swings will be applied.

Theory

The mass balance for a ZLC can be written as

$$M_S \frac{d\bar{n}}{dt} + V_F \frac{dc}{dt} = (Fc)_{IN} - (Fc)_{OUT} \quad (1)$$

Where c is the fluid phase concentration; $\bar{n}$ is the average adsorbed phase concentration; F is the volumetric flowrate at the temperature and pressure of the column; M_S is the mass of the solid in the column; and V_F is the volume of the fluid in the column, which can be measured from a blank experiment. During adsorption c_{IN} is the concentration of water coming from the bubbler, while in desorption $c_{IN} = 0$. As the ZLC behaves as a well mixed cell, $c_{OUT} = c$. Finally, due to adsorption and desorption the outlet volumetric flowrate will differ from the inlet value. It is possible to show that F can be calculated from the flowrate of the non-adsorbing carrier, F_{Carr}, and the measured concentration with sufficient accuracy for the case of water ($y_{bub} < 0.1$) using [20]

$$F = \frac{F_{Carr}}{1 - \frac{c}{c_{bub}} y_{bub}} \quad (2)$$

where c_{bub} and y_{bub} are the fluid phase concentration and mole fraction of the water coming from the bubbler.

An integral of the mass balance makes it possible to calculate the adsorbed phase concentration at any time

$$M_S(\bar{n} - \bar{n}_0) + V_F(c - c_0) = \int_0^t (Fc)_{IN} dt - \int_0^t (Fc)_{OUT} dt \quad (3)$$

Equation 3 is the basis for measuring equilibrium isotherms using low flowrates [21], which ensure that the fluid concentration is always at equilibrium with the adsorbed phase.

In adsorption $\bar{n}_0 = c_0 = 0$ and $(Fc)_{IN} = \frac{F_{Carr} c_{bub}}{1 - y_{bub}}$, therefore

$$M_S\bar{n} = \frac{F_{Carr}c_{bub}}{1-y_{bub}}t - \int_0^t (Fc)_{OUT}dt - V_F c \quad (4)$$

While in desorption $c_{IN} = 0$, $c_0 = c_{bub}$ and the integral of the mass balance can be used to determine the initial concentration at equilibrium

$$M_S\bar{n}_0 = \int_0^\infty (Fc)_{OUT}dt - V_F c_{bub} \quad (5)$$

giving

$$M_S\bar{n} = \int_0^\infty (Fc)_{OUT}dt - \int_0^t (Fc)_{OUT}dt - V_F c \quad (6)$$

In order to determine the mass transfer coefficient, the column mass balance is coupled to the mass balance in the particles

$$\frac{d\bar{n}}{dt} = ka\left(n_{Eq} - \bar{n}\right) \quad (7)$$

where a is the surface to volume ratio and n_{Eq} is the equilibrium concentration corresponding to the fluid concentration c. Therefore, the mass transfer coefficient is given by

$$ka = \frac{d\bar{n}}{dt}\Big/\left(n_{Eq} - \bar{n}\right) \quad (8)$$

It is useful to point out that in eq. 8 the mass of the sample appears in both the numerator and denominator. This means that for the determination of the mass transfer coefficient it is not necessary to measure accurately the mass of the dry sample.

The important result is that it is possible to obtain the mass transfer coefficient directly from a ZLC experiment without the need to use a model. n_{Eq} as a function of c is measured from low flowrate equilibrium experiments and correlated numerically, for example with cubic splines. $\bar{n}$ is calculated from the integral of the measured signal using eq. 3. Finally, rearranging eq. 1

$$M_S\frac{d\bar{n}}{dt} = (Fc)_{IN} - (Fc)_{OUT} - V_F\frac{dc}{dt} \quad (9)$$

which requires only the use of a piecewise smooth function to correlate the measured c as a function of time in order to determine $\frac{dc}{dt}$.

Experimental

The ZLC apparatus used in this study is described in detail in [22]. The water content in the carrier gas is controlled by adjusting, in the range 5-30 °C, the temperature of the bath in which a 100 ml bubbler is submerged. Two sets of Brooks mass flow controllers allow to operate the system under

low flow (equilibrium) and high flow (kinetic) conditions, maintaining the flowrates with an accuracy of 1.0% of rate (20–100% FS) and ±0.2% FS (below 20% FS) [22]. The experiment consists in flowing the pure carrier through the ZLC at a set flowrate and switching to the carrier and water mixture at the same flowrate (adsorption experiment) and after equilibration back to the pure carrier (desorption experiment). The concentration at the outlet of the ZLC is measured with an Ametek Dycor Dymaxion quadrupole mass spectrometer and a Rotronic HC2-SM humidity and temperature probe. The probe gives an accurate reading, ±0.8 %RH/±0.1 K, of the actual water concentration at equilibrium, c_{bub}, while the signal from the fast response mass spectrometer is converted to c/c_{bub} as a function of time.

The silica-gel used is a commercial sample from GeeJay Chemicals Ltd, which has an indicator that turns from bright orange (dry) to nearly transparent (wet) as water is adsorbed. As the beads are larger than the ID of a Swagelok 1/8" union used to house the sample, a fragment with a mass of 4.3 mg was cut from a bead and is shown in Fig. 1.

Figure 1. Detail of the silica-gel fragment housed in the ZLC.

The material consists of only pores below 10 nm as confirmed using a Quantachrome PoreMaster mercury porosimetry analyser. The intrusion/extrusion curves are reported in the Supplementary Materials. This measurement allows to determine also a density of the material of 1322 kg/m^3. The effective diameter of the fragment is therefore estimated to be 1.84 mm.

Prior to each set of experiments at a given temperature the sample was regenerated *in situ*. Before the first experiment and after each series of experiments the sample was heated at a rate of 1 °C/min up to 110 °C, held at this temperature for 1 hour, followed by a further temperature ramp at a rate of 1 °C/min up to 150 °C and held at this temperature for at least 6 hours.

Experiments at 25 °C were carried out at 1 and 1.5 cc/min in order to confirm equilibrium control. Figure 2 shows the isotherms calculated from the concentration signals using the mass balances described in the theory section.

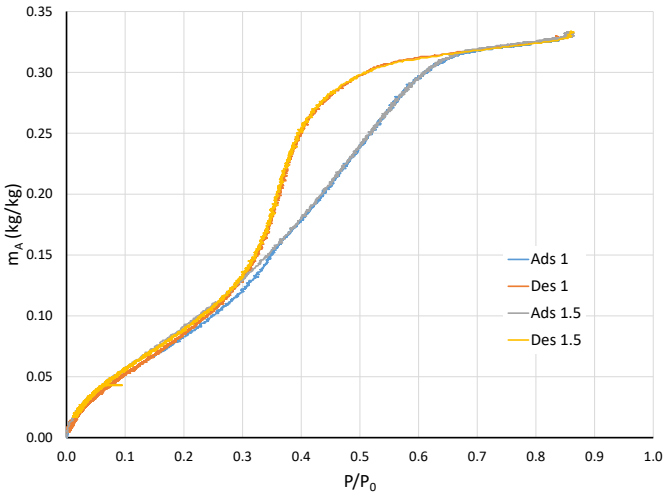

Figure 2. Adsorption and desorption isotherms at 25 °C using two flowrates.

The close agreement of the curves calculated from experiments at two flowrates confirms that already at 1.5 cc/min the system is under equilibrium control. As a result experiments at 10 °C and 40 °C were carried out only at 1 cc/min. The full set of isotherms measured at the 3 temperatures and 1 cc/min is shown in Figure 3. At 10 and 25 °C the range of temperatures available in the bubbler allows to operate the highest concentration above the closure of the hysteresis loop. At 40 °C the highest concentration is within the hysteresis loop and as a result the desorption branch is a scanning curve. The shape of the adsorption branch indicates that there is a broad distribution of mesopores. The fact that the desorption branch does not follow a path parallel to the adsorption branch indicates that pore connectivity is influencing the system [23,24]. For the purposes of this study though, given the large number of equilibrium points (>1000) for each branch, the equilibrium curves can be correlated by piece-wise smooth functions to interpolate values and obtain $\frac{n_{Eq}}{n_{Eqbub}}$ as a function of $\frac{c}{c_{bub}}$, dividing the measured isotherms by the endpoints.

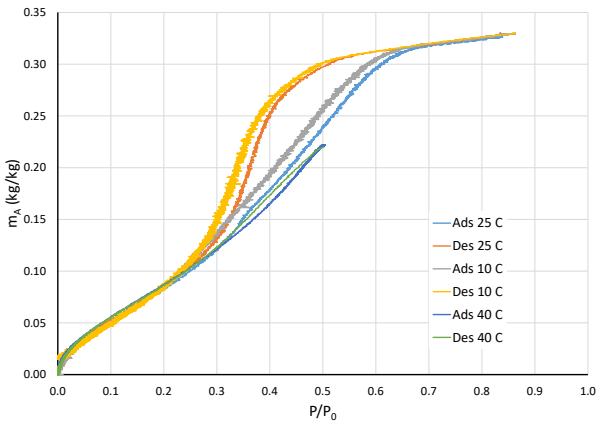

Figure 3. Adsorption and desorption isotherms at 10, 25 and 40 °C.

Results and discussion

The main aim of this contribution is to demonstrate the methodology to obtain directly the mass transfer coefficient from ZLC measurements without the need of a model. The most important assumption that is made is that the system remains isothermal, which is typically the case in a ZLC system [18] for 2 reasons: the first is due to the fact that a very small sample is housed in contact with a large mass of steel; the second is that all of the gas flows through the column providing additional convective heat transfer, thus limiting the temperature rise in adsorption and the temperature drop in desorption. A check of the worst case scenario can be carried out to estimate the maximum temperature rise estimating the Nusselt number for an isolated sphere using literature values of the heat capacity [13,25] and the energy of adsorption [13]. Experimentally a simple check is through a change in carrier gas, which will vary the heat transfer coefficient.

At 25 °C experiments at 11, 22, 33 cc/min (measured at room temperature) were performed. The concentration signals were then used to calculate the mass transfer coefficients. Figure 4 shows the results for the highest flowrate, which is also the experiment furthest from equilibrium. Similar results are obtained for the other two flowrates, indicating that the mass transfer coefficient is independent of flowrate. The figures for 11 and 22 cc/min are included in the Supplementary Materials.

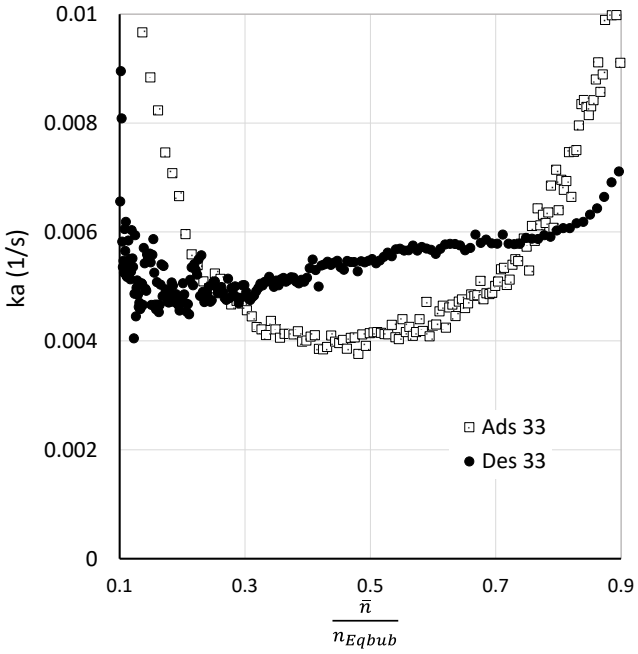

Figure 4. Mass transfer coefficient at 25 °C and 33 cc/min as a function of the reduced adsorbed phase concentration.

Points below $\frac{\bar{n}}{n_{Eqbub}}$ values of 0.1 and above 0.9 in Fig. 4 are not shown because the denominator in eq. 8 is very close to 0 and therefore the calculated coefficients are subject to larger uncertainties, which are becoming apparent for the desorption curve below $\frac{\bar{n}}{n_{Eqbub}} = 0.2$.

From Fig. 4 it is possible to observe that in desorption the mass transfer coefficient is mildly dependent on concentration, while in adsorption it has a minimum close to where the isotherm has the inflection corresponding to multilayer adsorption and condensation in the mesopores. The lack of symmetry would suggest that there is an internal diffusion process under adsorption conditions, which would explain the observed concentration dependence. A different process is observed in desorption, most likely a pore network effect as in the desorption branch of the isotherm. A detailed investigation of this complex behaviour is beyond the scope of the present study, but we note that for the purposes of representing adsorption and desorption kinetics Fig. 4 would suggest that an average mass transfer coefficient would be a reasonable approximation also in adsorption. Figure 5 shows the adsorption and desorption curves along with the predicted responses using $ka = 0.0049$ s^{-1} for all flowrates.

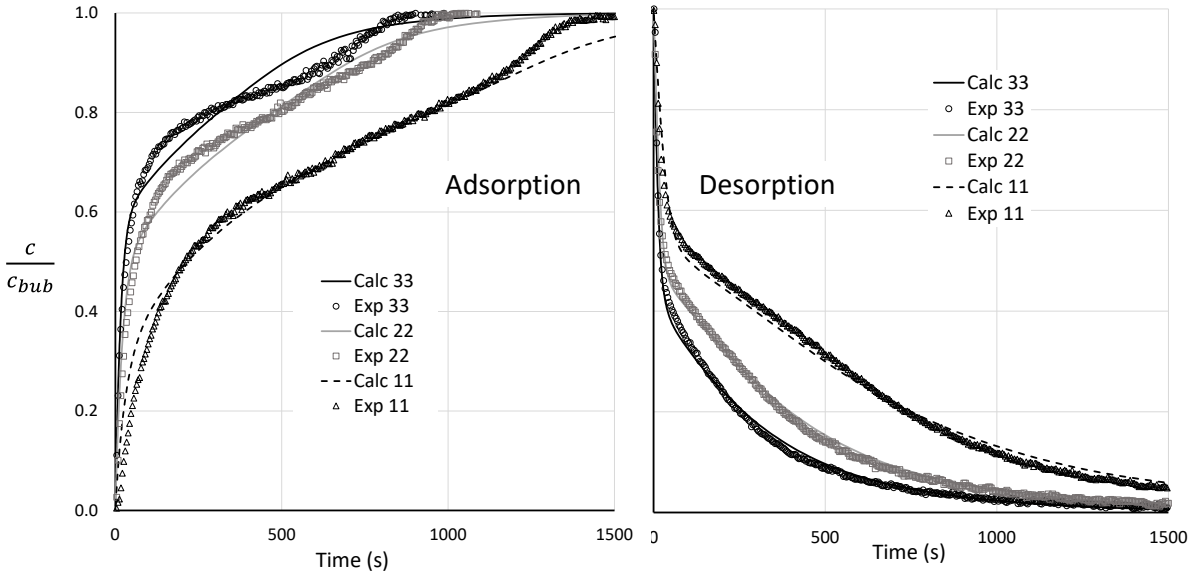

Figure 5. Adsorption and desorption kinetics at 25 °C and different flowrates. Calculated curves with $ka = 0.0049$ s^{-1}

At all flowrates the constant mass transfer coefficient provides an excellent match to the desorption curves. Only at 11 cc/min some slight deviation is observed. Similar arguments can be made for the adsorption curves, which show a more complex behaviour at all flowrates, but the simple model captures the overall kinetics.

Table 1: Mass transfer coefficients for water on silica-gel at 25 °C

ka at 25 °C, s^{-1}	Technique	Methodology	Sample size	Source
0.0049	ZLC	Integral step	< 10 mg Single bead	This work
$0.0149 - 0.0357$	Concentration-swing frequency response	Differential step	< 10 mg Single bead	[15]
$0.0009 - 0.0016$	Breakthrough	Integral step	> 10 g Bed of beads	[13]
0.0064	Gravimetric	Integral step	1 g Bed of beads	[26,27]

In Table 1, the mass transfer coefficient obtained in this study is compared to values reported in literature at similar conditions. Very similar mass transfer coefficients for water on silica-gel using large concentration swings that include the hysteresis loop have been used in the simulation of air drying using pressure swing adsorption [26,27]. A recent study based on modelling breakthrough curves [13] gives lower values by a factor of approximately 5, but still of a similar order of magnitude.

In the literature only a frequency response study [15] measured adsorption kinetics on a single particle of silica-gel and found that the linear driving force model provided a good representation of this system, with a mass transfer coefficient approximately 3 to 7 times the value found here. It is important to consider, though, that in a frequency response experiment both adsorption and desorption are sampled over a small concentration range and within the hysteresis loop the trajectory is on the scanning curve [15], not the actual adsorption or desorption branches.

Given the variability in silica-gel samples, see for example [25], these comparisons represent a very reasonable agreement with the results obtained here, providing a strong validation to the novel approach presented.

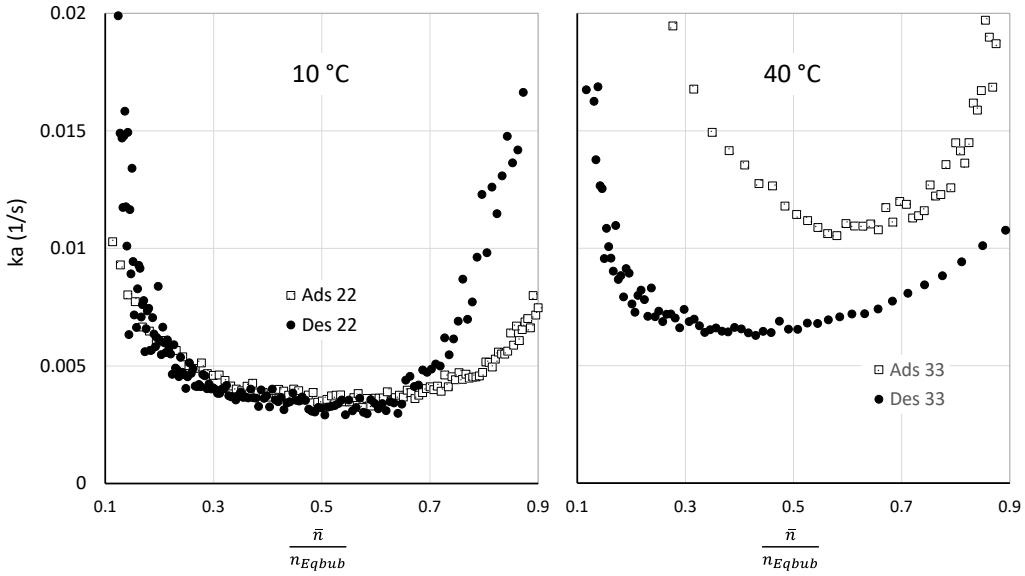

Figure 6. Mass transfer coefficient at 10 and 40 °C and as a function of the reduced adsorbed phase concentration.

Figure 6 shows the results obtained at 10 and 40 °C, where the corresponding average mass transfer coefficient values were found to be $ka = 0.0033$ s^{-1} and $ka = 0.0071$ s^{-1} respectively. These values, combined with the result at 25 °C, allow to estimate an activation energy of 19 kJ/mol, which is slightly less than half the latent heat of vaporization of water and similar to the activation energy found in large mesopore silica-gels [28]. The activation energy is consistent with surface diffusion as the main contribution as macro- and meso-pore diffusion without surface diffusion effects would show an apparent activation energy closer to the energy of adsorption [29]. For the silica-gel used in this study the adsorption energy is close to the latent heat of vaporization given that the isotherms shown in Fig. 2 are only slightly apart.

As a final validation of the interpretation of the kinetic responses, experiments were carried out with helium to determine if the mass transfer coefficient is independent of the carrier gas. Using the limiting value of 2 for the Sherwood number it is possible to estimate that the external film resistance is negligible in this system, in agreement with similar assessments in the literature [13]. For both carrier gases it is possible to the estimate that the Knudsen number is greater than 6 for the largest pores detected in appreciable amount by mercury porosimetry (10 nm), thus transport should only be a combination of Knudsen flow and surface diffusion. We note that in this case the mass transfer coefficient should be the same in a ZLC experiment and in a system with only water vapour present. Figure 7 shows the comparison of the adsorption and desorption results with the two carrier gases at 25 °C and the highest flowrate of 33 cc/min. The desorption curve shows a small

difference between the two experiments in the initial stages, where the response in helium indicates a larger mass transfer coefficient, followed by convergence to the same rate after the first 250 s.

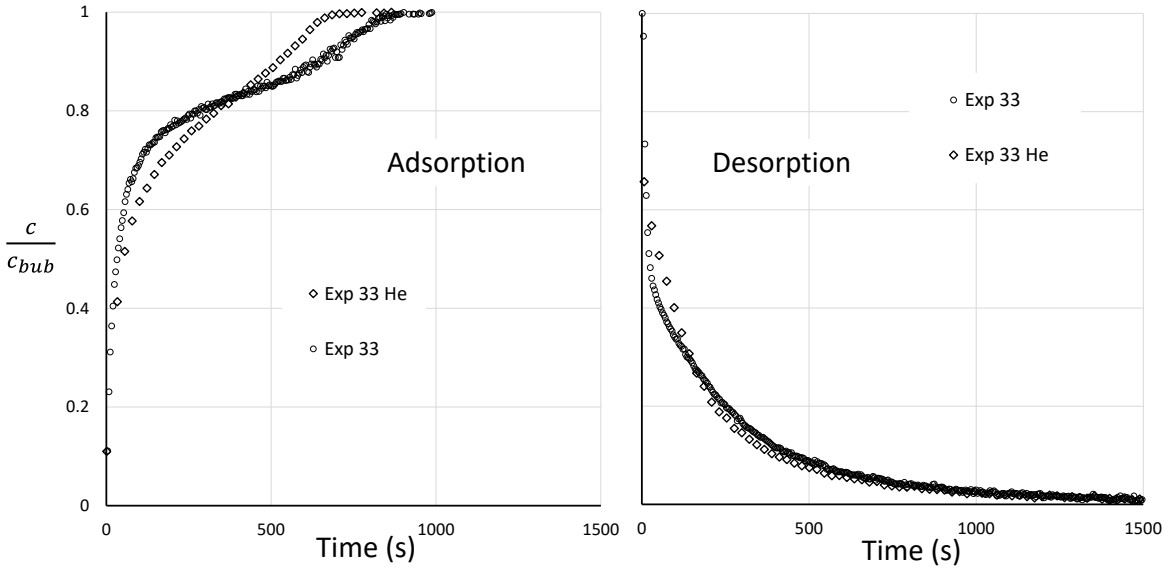

Figure 7. Adsorption and desorption kinetics at 25 °C and with nitrogen and helium as carrier gases.

For the adsorption curves there is a more pronounced effect, indicating a faster kinetic process with helium, particularly in the initial stages. This may indicate either that within the silica-gel particle there are fractures that do not result in appreciable pore volumes in the mercury intrusion measurements, which do contribute to the overall mass transfer kinetics, or that in the initial stages where the rate of water exchange is high the system deviates from isothermal conditions. An estimate of the maximum temperature swing for helium, assuming no contributions from the metal components of the ZLC and Nu = 5 (highest flowrate), is shown in Figure 8.

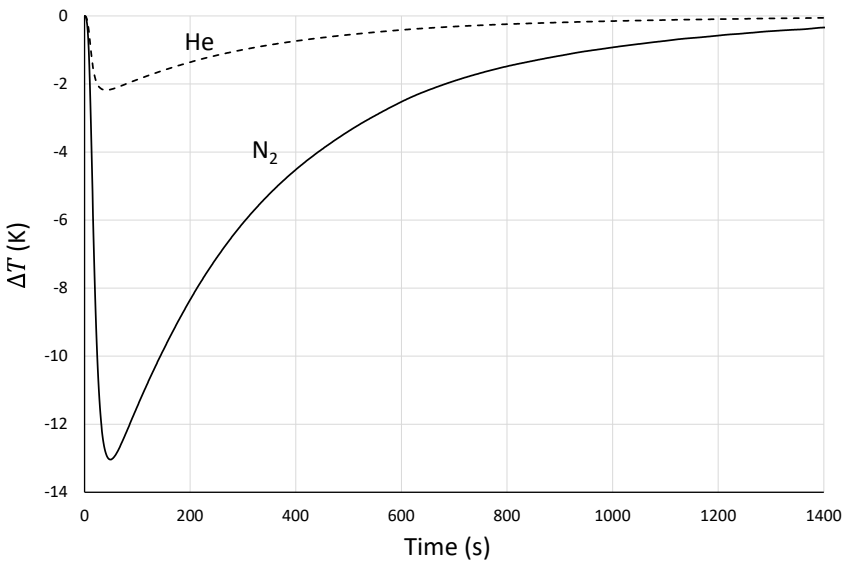

Figure 8. Predicted particle temperature change in desorption at 25 °C and 33 cc/min.

The predicted maximum temperature change with helium is 2 K in the initial 100 s of desorption, rapidly returning to near isothermal conditions by 200 s, indicating that even in this worst-case scenario this experiment is very close to isothermal conditions. The maximum temperature swing for nitrogen is estimated at 13 K, indicating that in this case care should be taken and suggesting that with nitrogen a ZLC experiment with silica-gel should be carried out with a reduced mass of 1-2 mg as the condition for isothermal behaviour is proportional to the square of the particle diameter [18,30]. The actual measured difference between the two gases is relatively small, indicating that the thermal mass is larger due to the contribution of the metal components, confirming that the helium experiment is effectively isothermal.

Conclusions

The methodology for the determination of the mass transfer coefficient of water in silica-gel using the zero length column experiment has been demonstrated for both adsorption and desorption steps. Using low flowrate experiments to determine the equilibrium isotherms, all elements needed for the determination of the mass transfer coefficients are available from experiments at high flowrates. The approach is unique since it allows to determine the mass transfer coefficient as a function of the adsorbed phase concentration in a single experiment without relying on any model and without the need to couple heat and mass transfer. Once the flowrate required to achieve equilibrium conditions is known, the method requires approximately one day to determine the equilibrium isotherm and a further day to obtain adsorption and desorption results at two different flowrates. This is very efficient, considering that gravimetric and volumetric experiments will require several days to determine more than 20 points on each branch of the isotherm and the interpretation of the corresponding kinetic experiments is not as straightforward.

The results obtained on a commercial silica-gel fragment show a complex behaviour. Integral desorption experiments are well represented by an average mass transfer coefficient, $ka = 0.0049$ s^{-1} at 25 °C, with an activation energy of 19 kJ/mol. Adsorption experiments show a more pronounced concentration dependence, which shows a minimum at the inflection point of the isotherm. This is potentially an indication of an internal diffusion process. The asymmetry in the kinetic response would suggest that desorption is limited by pore network effects, which are consistent with the shape of the hysteresis loop. The Knudsen number for the largest pores in the

silica-gel sample is greater than 6, but a small dependence on the carrier gas was observed when using nitrogen and helium. This could indicate either the presence of fractures within the silica-gel particle or deviation from isothermal conditions in the initial stages of the kinetic curves where the rate of exchanges is highest. A simple analysis predicting the maximum temperature swings in desorption indicates that the helium experiment is effectively isothermal, while with nitrogen a smaller sample mass of 1-2 mg would be recommended for the system water/silica-gel.

Acknowledgements

Financial support from the Engineering and Physical Sciences Research Council, under the grant Versatile Adsorption Processes for the Capture of Carbon Dioxide from Industrial Sources – FlexICCS (EP/N024613/1), is gratefully acknowledged.

Notation

a	Surface to volume ratio of solid, m^{-1}
c	Concentration in the fluid phase, mol m^{-3}
$\bar{c}$	Average concentration in the fluid phase, mol m^{-3}
c_0	Initial concentration in the fluid phase, mol m^{-3}
c_{bub}	Fluid concentration in the fluid phase from the bubbler, mol m^{-3}
F	Volumetric flowrate, m^3 s^{-1}
F_{Carr}	Volumetric flowrate of carrier gas, m^3 s^{-1}
k	Surface mass transfer resistance, m s^{-1}
M_S	Mass of sample, kg
$\bar{n}$	Average concentration in the adsorbed phase, mol m^{-3}
$\bar{n}_0$	Initial concentration in the adsorbed phase, mol m^{-3}
n_{Eq}	Adsorbed phase concentration at equilibrium with c, mol m^{-3}
n_{Eqbub}	Adsorbed phase concentration at equilibrium with c_{bub}, mol m^{-3}
t	Time, s
V_F	Volume of fluid, m^3
y_{bub}	Mole fraction in the fluid phase from the bubbler

References

[1] Alsaman AS, Askalany AA, Harby K, Ahmed MS. Performance evaluation of a solar-driven adsorption desalination-cooling system. Energy 2017;128:196–207. https://doi.org/10.1016/j.energy.2017.04.010.

[2] Frazzica A, Brancato V, Caprì A, Cannilla C, Gordeeva LG, Aristov YI. Development of "salt in porous matrix" composites based on LiCl for sorption thermal energy storage. Energy 2020;208:118338. https://doi.org/10.1016/j.energy.2020.118338.

[3] Gordeeva LG, Aristov YI. Adsorptive heat storage and amplification: New cycles and adsorbents. Energy 2019;167:440–53. https://doi.org/10.1016/j.energy.2018.10.132.

[4] Grabowska K, Sztekler K, Krzywanski J, Sosnowski M, Stefanski S, Nowak W. Construction of an innovative adsorbent bed configuration in the adsorption chiller part 2. experimental research of coated bed samples. Energy 2021;215:119123. https://doi.org/10.1016/j.energy.2020.119123.

[5] Graf S, Eibel S, Lanzerath F, Bardow A. Validated Performance Prediction of Adsorption Chillers: Bridging the Gap from Gram-Scale Experiments to Full-Scale Chillers. Energy Technol 2020;8:1901130. https://doi.org/https://doi.org/10.1002/ente.201901130.

[6] Fong KF, Lee CK. Impact of adsorbent characteristics on performance of solid desiccant wheel. Energy 2018;144:1003–12. https://doi.org/10.1016/j.energy.2017.12.113.

[7] Wu XN, Ge TS, Dai YJ, Wang RZ. Investigation on novel desiccant wheel using wood pulp fiber paper with high coating ratio as matrix. Energy 2019;176:493–504. https://doi.org/10.1016/j.energy.2019.04.006.

[8] Baker FS, Sing KSW. Specificity in the adsorption of nitrogen and water on hydroxylated and dehydroxylated silicas. J Colloid Interface Sci 1976;55:605–13. https://doi.org/10.1016/0021-9797(76)90071-0.

[9] Naono H, Fujiwara R, Yagi M. Determination of physisorbed and chemisorbed waters on silica gel and porous silica glass by means of desorption isotherms of water vapor. J Colloid Interface Sci 1980;76:74–82. https://doi.org/10.1016/0021-9797(80)90272-6.

[10] Rajniak P, Yang RT. A simple model and experiments for adsorption-desorption hysteresis: Water vapor on silica gel. AIChE J 1993;39:774–86. https://doi.org/https://doi.org/10.1002/aic.690390506.

[11] Sarkisov L, Centineo A, Brandani S. Molecular simulation and experiments of water adsorption in a high surface area activated carbon: Hysteresis, scanning curves and spatial organization of water clusters. Carbon N Y 2017;118:127–38. https://doi.org/10.1016/j.carbon.2017.03.044.

[12] Velasco LF, Guillet-Nicolas R, Dobos G, Thommes M, Lodewyckx P. Towards a better understanding of water adsorption hysteresis in activated carbons by scanning isotherms. Carbon N Y 2016;96:753–8. https://doi.org/10.1016/j.carbon.2015.10.017.

[13] Goyal P, Purdue MJ, Farooq S. Adsorption and diffusion of moisture and wet flue gas on silica gel. Chem Eng Sci 2020;227:115890. https://doi.org/10.1016/j.ces.2020.115890.

[14] Hossain MI, Glover TG. Kinetics of Water Adsorption in UiO-66 MOF. Ind Eng Chem Res 2019;58:10550–8. https://doi.org/10.1021/acs.iecr.9b00976.

[15] Glover TG, Wang Y, LeVan MD. Diffusion of Condensable Vapors in Single Adsorbent Particles

Measured via Concentration-Swing Frequency Response. Langmuir 2008;24:13406–13. https://doi.org/10.1021/la802222r.

[16] Aristov YI. Dynamics of adsorptive heat conversion systems: Review of basics and recent advances. Energy 2020;205:117998. https://doi.org/10.1016/j.energy.2020.117998.

[17] Hefti M, Joss L, Marx D, Mazzotti M. An Experimental and Modeling Study of the Adsorption Equilibrium and Dynamics of Water Vapor on Activated Carbon. Ind Eng Chem Res 2015;54:12165–76. https://doi.org/10.1021/acs.iecr.5b03445.

[18] Brandani S, Mangano E. The zero length column technique to measure adsorption equilibrium and kinetics: lessons learnt from 30 years of experience. Adsorption 2021;27:319–51. https://doi.org/10.1007/s10450-020-00273-w.

[19] Eic M, Ruthven DM. A new experimental technique for measurement of intracrystalline diffusivity. Zeolites 1988;8:40–5. https://doi.org/10.1016/S0144-2449(88)80028-9.

[20] Wang H, Brandani S, Lin G, Hu X. Flowrate correction for the determination of isotherms and Darken thermodynamic factors from Zero Length Column (ZLC) experiments. Adsorption 2011;17:687–94. https://doi.org/10.1007/s10450-011-9364-0.

[21] Brandani F, Ruthven D, Coe CG. Measurement of Adsorption Equilibrium by the Zero Length Column (ZLC) Technique Part 1: Single-Component Systems. Ind Eng Chem Res 2003;42:1451–61. https://doi.org/10.1021/ie020572n.

[22] Centineo A, Brandani S. Measurement of water vapor adsorption isotherms in mesoporous materials using the zero length column technique. Chem Eng Sci 2020;214:115417. https://doi.org/10.1016/j.ces.2019.115417.

[23] Lowell S, Shields JE, Thomas MA, Thommes M. Characterization of Porous Solids and Powders: Surface Area, Pore Size and Density. vol. 16. Dordrecht: Springer Netherlands; 2004. https://doi.org/10.1007/978-1-4020-2303-3.

[24] Thommes M, Kaneko K, Neimark A V, Olivier JP, Rodriguez-Reinoso F, Rouquerol J, et al. Physisorption of gases, with special reference to the evaluation of surface area and pore size distribution (IUPAC Technical Report). Pure Appl Chem 2015;87:1051–69. https://doi.org/doi:10.1515/pac-2014-1117.

[25] Islam MA, Pal A, Saha BB. Experimental study on thermophysical and porous properties of silica gels. Int J Refrig 2020;110:277–85. https://doi.org/10.1016/j.ijrefrig.2019.10.027.

[26] Štěpánek F, Kubíček M, Marek M, Šoóš M, Rajniak P, Yang RT. On the modeling of PSA cycles with hysteresis-dependent isotherms. Chem Eng Sci 2000;55:431–40. https://doi.org/10.1016/S0009-2509(99)00338-3.

[27] Chihara K, Suzuki M. Air drying by pressure swing adsorption. J Chem Eng JAPAN 1983;16:293–9. https://doi.org/10.1252/jcej.16.293.

[28] Li X, Li Z, Xia Q, Xi H. Effects of pore sizes of porous silica gels on desorption activation energy of water vapour. Appl Therm Eng 2007;27:869–76. https://doi.org/10.1016/j.applthermaleng.2006.09.010.

[29] Kärger J, Ruthven DM, Theodorou DN. Diffusion in Nanoporous Materials. Weinheim, Germany: Wiley-VCH Verlag GmbH & Co. KGaA; 2012. https://doi.org/10.1002/9783527651276.

[30] Brandani S, Cavalcante C, Guimarães A, Ruthven D. Heat Effects in ZLC Experiments. Adsorption 1998;4:275–85. https://doi.org/10.1023/A:1008837801299.